

---

# PINNFLUENCE: INFLUENCE FUNCTIONS FOR PHYSICS-INFORMED NEURAL NETWORKS

---

Jonas R. Naujoks<sup>1,\*</sup>  
Thomas Wiegand<sup>1,2,3</sup>

Aleksander Krasowski<sup>1,\*</sup>  
Sebastian Lapuschkin<sup>1</sup>  
René P. Klausen<sup>1,†</sup>

Moritz Weckbecker<sup>1</sup>  
Wojciech Samek<sup>1,2,3,†</sup>

<sup>1</sup>Fraunhofer HHI, 10587 Berlin, Germany

<sup>2</sup>Technische Universität Berlin, 10587 Berlin, Germany

<sup>3</sup>BIFOLD – Berlin Institute for the Foundations of Learning and Data, 10587 Berlin, Germany

<sup>†</sup>corresponding authors: {wojciech.samek, rene.pascal.klausen}@hhi.fraunhofer.de

\*equal contribution.

## ABSTRACT

Recently, physics-informed neural networks (PINNs) have emerged as a flexible and promising application of deep learning to partial differential equations in the physical sciences. While offering strong performance and competitive inference speeds on forward and inverse problems, their black-box nature limits interpretability, particularly regarding alignment with expected physical behavior. In the present work, we explore the application of influence functions (IFs) to validate and debug PINNs post-hoc. Specifically, we apply variations of IF-based indicators to gauge the influence of different types of collocation points on the prediction of PINNs applied to a 2D Navier-Stokes fluid flow problem. Our results demonstrate how IFs can be adapted to PINNs to reveal the potential for further studies.

## 1 Introduction

Time and time again, deep learning approaches have proven themselves to be exceptionally capable at solving problems that were considered hard and time-consuming, yielding fast inference times bundled with strong performance. Physics-informed neural networks (PINNs) [23] represent another recent iteration of that trend applied to the realm of partial differential equations (PDEs). By incorporating prior physical knowledge in the form of differential equations [6; 9; 10; 23], they admit a wide range of possible applications such as fluid mechanics, electromagnetics, disease modelling and optics, inter alia [1; 2; 4; 19]. Despite the power of PINNs, there remains the challenge of understanding and improving model behavior when things go wrong [15; 25; 26]. PINNs minimize complex composite losses, which complicates the tracing of poor performance to specific training points or conditions; this is the main motivation for this work.

Influence functions [12] (IFs) systematically assess the contribution of individual training points to a model’s behavior. Recent studies have shown that incorporating physical concepts like temporal causality improves PINN performance [7; 28], highlighting the role of underlying physical principles. By identifying key points, such as those near boundaries or critical regions, we can assess whether the PINN’s learned parameters align with the physics of the problem. For many PDEs, practitioners possess an intuitive understanding of the underlying physics. For example, in magnetostatics, the magnetic field is fundamentally generated by source terms. A well-trained PINN could be expected to reflect this relation. We aim to show how domain experts can use this approach to validate the model by identifying key training points, boundary conditions or physical principles that have the greatest impact on the model’s behavior. This also allows them to estimate the effect of inductive biases and observed data on the model’s predictions. Notably, PINNs also provide a powerful application domain for IFs and other data attribution methods, as models and datasets are usually much smaller than those used in computer vision or natural language processing. This makes calculation of IFs computationally feasible, and the effect of individual data points on the fit of the model is expected to be greater.

**Our Contributions** (i) We adapt influence functions to PINNs as a tool for improving their interpretability. (ii) In addition, we derive heuristically motivated indicators based on influence functions to showcase how they can be leveraged by domain-knowledgeable users to test and validate PINNs. (iii) We empirically demonstrate their usefulness in disambiguating between three different versions of PINNs applied to a Navier-Stokes problem.

## 2 Theoretical Background

**Physics-Informed Neural Networks** introduced in [23], constitute a machine-learning-based approach to solving partial differential equations (PDEs), which are ubiquitous in physical sciences. Let  $\Omega \subseteq \mathbb{R}^n$  be an open domain and consider the initial boundary value problem (IBVP)

$$\begin{aligned}\mathcal{N}[u](\mathbf{x}) &= 0, & \mathbf{x} \in \Omega \\ \mathcal{B}[u](\mathbf{x}) &= 0, & \mathbf{x} \in \partial\Omega\end{aligned}\quad (1)$$

Here,  $\mathcal{N}$  and  $\mathcal{B}$  are differential operators acting on the solution of the PDE  $u : \Omega \rightarrow \mathbb{R}^d$ , where  $\mathbf{x}$  typically represents the spatial as well as possible temporal coordinates. Note that Eq. (2) is formulated to capture i.a. Dirichlet as well as von-Neumann conditions.

The goal of PINNs is to approximate the solution of a given differential equation using a neural network  $\phi(\mathbf{x}; \theta)$ , which depends on parameters  $\theta \in \Theta$  and an input  $\mathbf{x}$ . These parameters are optimized by training  $\phi$  using a composite loss function, consisting of the PDE residual and boundary conditions  $\mathcal{L} = \mathcal{L}_{\text{pde}} + \mathcal{L}_{\text{bc}}$ , with  $\mathcal{L}_{\text{pde}} = \frac{1}{N_{\text{pde}}} \sum_{i=1}^{N_{\text{pde}}} |\mathcal{N}[\phi(\mathbf{x}_i; \theta)]|^2$ ,  $\mathcal{L}_{\text{bc}} = \frac{1}{N_{\text{bc}}} \sum_{i=1}^{N_{\text{bc}}} |\mathcal{B}[\phi(\mathbf{x}_i; \theta)]|^2$ , and where  $N_{\text{pde}}$  as well as  $N_{\text{bc}}$  are the numbers of randomly sampled collocation from  $\Omega$  and  $\partial\Omega$ , respectively. Note that one can also consider a data-driven regression loss, which we drop for the sake of simplicity.

**Influence Functions** The question being addressed by influence functions [5; 8; 12] is *how would the model’s behavior change if certain training points were not present in the training set?* By linearly approximating the effect of leave-one-out retraining, IFs provide a possibility of studying a model through the lens of its training data. In order to adapt the influence functions to PINNs we will slightly generalize the approach of [12; 13]. We provide a full derivation and proof, including details on all necessary assumptions, in Appendix A.1. Suppose we have trained a model by minimizing a loss  $\frac{1}{N} \sum_i L(\mathbf{x}_i; \theta)$  on a training data set  $\mathcal{X} = \{\mathbf{x}_1, \dots, \mathbf{x}_N\}$  and derived an optimal parameter  $\hat{\theta} \in \Theta$ . Furthermore, consider a function  $f : \Omega \times \Theta \rightarrow \mathbb{R}$ , which depends on the parameter  $\theta \in \Theta$  and some other parameter  $\mathbf{z} \in \Omega$  (such as in [12], the loss  $L$  for a single test point  $\mathbf{z}$ ). We now aim to approximate  $f(\mathbf{z}; \hat{\theta}^+) - f(\mathbf{z}; \hat{\theta})$  if  $\hat{\theta}^+$  were optimized over an amended training data set that includes an additional training point  $\mathbf{x}^+$ . This can be approximated by

$$\text{Inf}_{f(\mathbf{z}; \hat{\theta})}(\mathbf{x}^+) := \nabla_{\hat{\theta}} f(\mathbf{z}; \hat{\theta}) \cdot H_{\hat{\theta}}^{-1} \cdot \nabla_{\hat{\theta}} L(\mathbf{x}^+; \hat{\theta}) \quad , \quad (3)$$

where  $H_{\hat{\theta}} = \nabla_{\hat{\theta}}^2 \frac{1}{N} \sum_{i=1}^N L(\mathbf{x}_i; \theta)$  denotes the Hessian. This approach can be extended to the addition and removal of multiple training data points: Let  $\mathcal{X}^+ = \{\mathbf{x}_1^+, \dots, \mathbf{x}_{m^+}^+\}$  be the set of training points we want to add and  $\mathcal{X}^- = \{\mathbf{x}_1^-, \dots, \mathbf{x}_{m^-}^-\} \subseteq \mathcal{X}$  the set we want to remove from our training set. The effect of retraining the model with added and removed training points can then be approximated by  $\text{Inf}_{f(\mathbf{z}; \hat{\theta})}(\mathcal{X}^+, \mathcal{X}^-) := \sum_{i=1}^{m^+} \text{Inf}_{f(\mathbf{z}; \hat{\theta})}(\mathbf{x}_i^+) - \sum_{i=1}^{m^-} \text{Inf}_{f(\mathbf{z}; \hat{\theta})}(\mathbf{x}_i^-)$ . Hence, we can study the influence of single sampling points as well as regions on loss functions, any type of predictions or derived quantities. By studying the influence resulting therefrom, one can compare the model’s behavior with physical intuition. Using this method, we can also estimate the effect of adding and removing entire loss terms for composite losses (see Corollary 1 in the appendix).

## 3 Experiments

**Navier-Stokes Problem** The Navier-Stokes equations describe the motion of viscous Newtonian fluids and represent the cornerstone of fluid dynamics. Consequently, they are widely used in various applications. In the present work, we focus on a laminar, incompressible and time-independent fluid flow around a cylinder in a rectangular cavity with open lateral boundaries in 2D [24], see Fig. 1. The stationary equations of motions as well as the continuity equation are given as follows:

$$(\mathbf{u} \cdot \nabla) \mathbf{u} + \frac{1}{\rho} \nabla p - \nu \nabla^2 \mathbf{u} = 0, \quad \text{div } \mathbf{u} = 0, \quad (4)$$

where  $\mathbf{u}(x, y) \in \mathbb{R}^2$  denotes the velocity field,  $p(x, y) \in \mathbb{R}$  represents the pressure,  $\rho$  is the density, and  $\nu$  is the kinematic viscosity. The domain is given by  $\Omega = (x_{\min}, x_{\max}) \times (y_{\min}, y_{\max}) \setminus C_r$ , with  $C_r$  denoting the cylinder with radius  $r$ . The boundary conditions at the bottom, top, and cylinder are given by  $\mathbf{u} = 0$ . The inflow condition on the left has a parabolic profile. For the rightward outflow condition, we use a directional "do nothing" condition [20]:  $\nu \nabla u_1(x_{\max}, y) - (\frac{p}{\rho}, 0)^\top = 0$ . The used parameters of the geometry and PDE are given in A.2. The task of the PINN is then to predict  $\mathbf{u}(x, y)$  and  $p(x, y)$ .

**Experimental Setup** We train fully-connected PINNs consisting of 4 layers with 64 nodes each with GELU activation functions and 3 outputs. These correspond to the solution of Eq. (4) that we want to predict:  $u_1$ ,  $u_2$  and  $p$ . For the training data set, we randomly draw  $N_{\text{pde}}$  points inside the domain  $\Omega$  and  $N_{\text{bc}}$  from the boundary using Hammersley sampling. In essence, these are pairs of  $(x, y)$  coordinates as we consider a 2D PDE. We train three models, (1) *good* model  $\phi_{\text{good}}$  with the correct PDE and  $N_{\text{pde}} = 7500$  and  $N_{\text{bc}} = 2500$  that solves the task well compared to a reference solution [27]; (2) a *broken* model  $\phi_{\text{broken}}$  with the same number of training points but with the  $(u_1 \cdot \nabla)u_1$  part of Eq. (4) missing, thus trained on wrong physics; (3) and a *bad* model  $\phi_{\text{bad}}$  with the correct PDE but with  $N_{\text{pde}} = 1500$  and  $N_{\text{bc}} = 500$ , such that it consequently performs badly. Each model is trained in two phases. First, Adam [11] is used as an optimizer for a total of 100k steps, followed by further refining the model parameter's using L-BFGS [17] for up to 25k steps. We slightly adapted the DeepXDE library [18] to allow for more fine-grained gradient manipulation while using PyTorch [21] as our backend. For the test set, we draw a total of 36934 points from  $\Omega$  and 1288 points from  $\partial\Omega$  [27]. The influences are calculated using the NaiveInfluenceFunction from captum [14].

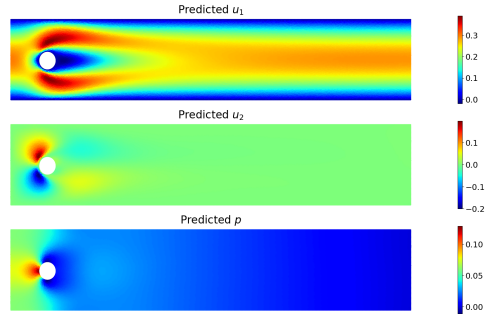


Figure 1: Trained model ( $\phi_{\text{good}}$ ) with predictions:  $u_1$ ,  $u_2$ ,  $p$  (top to bottom).

**Empirical Indicators** In this study, we aim to answer the following question using influence functions: *Can we identify or test whether the PINN has learned certain aspects of the underlying physical principles of the Navier-Stokes problem?* Since predictions alone do not reveal the influence of training data or boundary conditions, we devise a set of heuristic indicators.



Figure 2: Influence heatmap on the prediction of  $u_1$  of a single training point ( $\times$ ) close to the cylinder (bottom).

We propose two IF-based indicators that are designed to capture aspects of the physical processes inherent to the PDE (4) and to serve as exemplary metrics showcasing how expert users can design tests to validate PINNs against their prior knowledge of the problem. As a first indication metric, we concentrate on the flow direction of the Navier-Stokes problem: the inflow is given at the left boundary of the domain and the outflow lies on the juxtaposed side. Figure 2 shows the influence pattern of a training point close to the cylinder.

We thus test a model on whether its influence patterns reflect this behavior. To define the directional indicator (DI), which captures the relevance share associated with the collocation point  $\mathbf{x}_{\text{test}}$  on the test points that follow in the direction of the flow (i.e. having larger  $x$ -component), we write:

$$\text{DI}(\mathbf{x}_{\text{test}}) := \frac{\sum_{\mathbf{x}_{\text{train}}: x_{\text{train}} > x_{\text{test}}} \left| \text{Inf}_{f(\mathbf{x}_{\text{test}}; \hat{\theta})}(\mathbf{x}_{\text{train}}) \right|}{\sum_{\mathbf{x}_{\text{train}}} \left| \text{Inf}_{f(\mathbf{x}_{\text{test}}; \hat{\theta})}(\mathbf{x}_{\text{train}}) \right|} \in [0, 1] \quad (5)$$

A larger value of DI implies that a given test point mainly influences the prediction further down in the direction of the flow rather than before and implies that the model has learned this underlying physical phenomenon of directed flows.

As a second indicator, we are interested in the fraction of influence that is associated with a given object in the input domain. In the present Navier-Stokes problem, the cylinder plays a central role in the flow field: it obstructs the flow. Thus, the overall velocity and pressure fields should be heavily influenced by its position. To this end, we devise an object or region identifier, which is designed to capture the influence associated with a given object in the domain (in our case around the cylinder). For the object or region indicator (OI), which sums up the relevance of removing a region  $\Xi \subseteq \bar{\Omega}$ , we write:

$$\text{OI}(\Xi) := \frac{\sum_{\mathbf{x}_{\text{train}} \in \Xi} \left| \text{Inf}_{f(\mathbf{x}_{\text{test}}; \hat{\theta})}(\mathbf{x}_{\text{train}}) \right|}{\sum_{\mathbf{x}_{\text{train}}} \left| \text{Inf}_{f(\mathbf{x}_{\text{test}}; \hat{\theta})}(\mathbf{x}_{\text{train}}) \right|} \in [0, 1] \quad (6)$$

A higher value of OI means that the region in question, such as the cylinder in our case, has an increased influence on the prediction for all other points. This is to be expected for a model that aims to accurately reflect the physics. In this investigation, we choose  $\Xi = C_{1.5r}$ , meaning that we remove the area with a 1.5 times the radius of the cylinder, see Fig. 3.

**Results** We evaluate the three different iterations of PINNs on the Navier-Stokes task. Figures 3a to 3c show heatmaps of how influential individual training points were to the whole test set. For  $\phi_{\text{good}}$ , the most influential points are distributed close to the inflow, on the outflow and especially around the cylinder. This is expected, as these areas determine the fluid flow. Furthermore, we observe that for  $\phi_{\text{bad}}$ , the upper left boundary is overly influential. And finally,  $\phi_{\text{broken}}$ 's influences are again distributed well around the cylinder. In Table 1, the aggregated mean values of the indicators are presented. Both  $\phi_{\text{good}}$  and  $\phi_{\text{bad}}$  show stronger DI performance. This suggests that both models have successfully learned to capture the dependence of the fluid flow on preceding points. When it comes to the OI indicator, this trend is even clearer. Here, the good model achieves superior performance, which suggests that the cylinder here has the biggest absolute influence, reflecting its importance for the fluid flow. It is important to note that these indicators are tools for investigating model behavior. Performing well on an indicator does not imply that the model is entirely correct, but rather that it does not fail in the specific aspect the indicator evaluates. Expert knowledge is essential for designing meaningful indicators, and further investigation is needed to validate their robustness. Additionally, if the indicator's assumptions are flawed, the results may be misleading and fail to provide sensible insights.

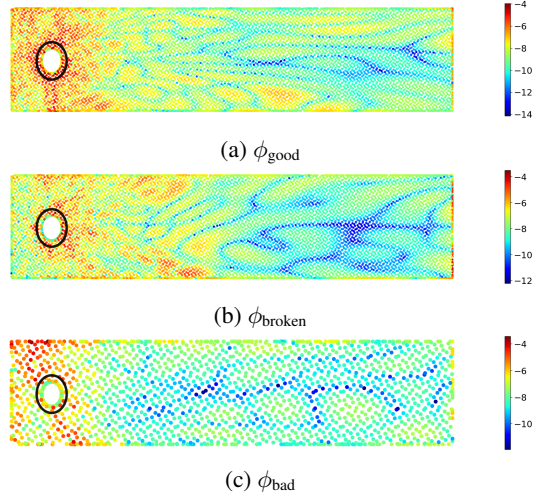


Figure 3: Average log values of  $|\text{Inf}_{\sum_i \|u(\mathbf{x}_i; \theta)\|}(\mathbf{x})|$  over the domain  $\bar{\Omega}$ . The area of  $C_{1.5r}$  is outlined in black.

## 4 Conclusion

We showcased how influence functions can help to evaluate PINNs. In particular, we formulated heuristically motivated indicators designed to test certain physical concepts. By applying this method to a Navier-Stokes problem, we observed that the best-performing model consistently aligned with these indicators, confirming their utility in assessing model performance. Still, further exploration of IF-based markers is indicated to rigorously validate the broad applicability of the presented approach. Using influence functions to improve PINN training through methods like resampling training points [16], enforcing temporal causality [28], or dynamically reweighing loss terms [3] – combined with IF-based training time techniques like TracIN [22] – presents a promising direction for future research. Additionally, further studies on the influence on parts of the loss as well as on different physical quantities, e.g. the vorticity, appears to be a logical next step.

Table 1: Mean values for the Direction  $\overline{\text{DI}}$  and Region  $\overline{\text{OI}}$  Indicators, aggregated over all  $\mathbf{x}_{\text{test}}$ . A higher score indicates a closer alignment with the indicator's assumptions.

$f(x, \theta)$	$\overline{\text{DI}}$			$\overline{\text{OI}}(C_{1.5r})$		
	$\phi_{\text{good}}$	$\phi_{\text{bad}}$	$\phi_{\text{broken}}$	$\phi_{\text{good}}$	$\phi_{\text{bad}}$	$\phi_{\text{broken}}$
$u_1$	<b>0.8</b>	<b>0.8</b>	0.71	<b>0.23</b>	0.18	0.13
$u_2$	<b>0.82</b>	0.77	0.69	<b>0.26</b>	0.17	0.14
$p$	0.83	<b>0.87</b>	0.79	<b>0.28</b>	0.18	0.22
$\ u\ $	<b>0.8</b>	0.79	0.71	<b>0.23</b>	0.18	0.13
$\mathcal{L}_{\text{pde}}$	<b>0.79</b>	0.76	0.73	<b>0.21</b>	0.14	0.16
$\mathcal{L}_{\text{bc}}$	<b>0.75</b>	0.71	0.65	<b>0.25</b>	0.16	0.15
$\mathcal{L}$	<b>0.79</b>	0.76	0.73	<b>0.21</b>	0.14	0.16

## Acknowledgments

The authors want to thank Galip Ümit Yolcu for fruitful discussions. This work was supported by the Fraunhofer Internal Programs under Grant No. PREPARE 40-08394.

## Code Availability

The code is available at <https://github.com/aleks-krasowski/PINNfluence>.

## References

- [1] Andrés Beltrán-Pulido, Ilias Bilionis, and Dionysios Aliprantis. Physics-informed neural networks for solving parametric magnetostatic problems. *IEEE Transactions on Energy Conversion*, 37(4):2678–2689, December 2022. arXiv:2202.04041 [physics].
- [2] Sarah Berkhahn and Matthias Ehrhardt. A physics-informed neural network to model COVID-19 infection and hospitalization scenarios. *Advances in Continuous and Discrete Models*, 2022(1):61, October 2022.
- [3] Rafael Bischof and Michael Kraus. Multi-Objective Loss Balancing for Physics-Informed Deep Learning. 2021. arXiv:2110.09813 [cs].
- [4] Shengze Cai, Zhiping Mao, Zhicheng Wang, Minglang Yin, and George Em Karniadakis. Physics-informed neural networks (PINNs) for fluid mechanics: A review, May 2021. arXiv:2105.09506 [physics].
- [5] R. Dennis Cook and Sanford Weisberg. *Residuals and Influence in Regression*. New York: Chapman and Hall, 1982.
- [6] Salvatore Cuomo, Vincenzo Schiano Di Cola, Fabio Giampaolo, Gianluigi Rozza, Maziar Raissi, and Francesco Piccialli. Scientific Machine Learning Through Physics-Informed Neural Networks: Where we are and What’s Next. *Journal of Scientific Computing*, 92(3):88, September 2022.
- [7] Jia Guo, Haifeng Wang, Shilin Gu, and Chenping Hou. TCAS-PINN: Physics-informed neural networks with a novel temporal causality-based adaptive sampling method. *Chinese Physics B*, 33(5):050701, April 2024. Publisher: Chinese Physical Society and IOP Publishing Ltd.
- [8] Frank R. Hampel. The Influence Curve and its Role in Robust Estimation. *Journal of the American Statistical Association*, 69(346):383–393, June 1974.
- [9] George Em Karniadakis, Ioannis G. Kevrekidis, Lu Lu, Paris Perdikaris, Sifan Wang, and Liu Yang. Physics-informed machine learning. *Nature Reviews Physics*, 3(6):422–440, May 2021.
- [10] Sung Wook Kim, Iljeok Kim, Jonghwan Lee, and Seungchul Lee. Knowledge Integration into deep learning in dynamical systems: an overview and taxonomy. *Journal of Mechanical Science and Technology*, 35(4):1331–1342, April 2021.
- [11] Diederik P. Kingma and Jimmy Ba. Adam: A Method for Stochastic Optimization, January 2017. arXiv:1412.6980 [cs].
- [12] Pang Wei Koh and Percy Liang. Understanding Black-box Predictions via Influence Functions, December 2020. arXiv:1703.04730 [cs, stat].
- [13] Pang Wei Koh, Kai-Siang Ang, Hubert H. K. Teo, and Percy Liang. On the Accuracy of Influence Functions for Measuring Group Effects, November 2019. arXiv:1905.13289 [cs, stat].
- [14] Narine Kokhlikyan, Vivek Miglani, Miguel Martin, Edward Wang, Bilal Alsallakh, Jonathan Reynolds, Alexander Melnikov, Natalia Kliushkina, Carlos Araya, Siqi Yan, and Orion Reblitz-Richardson. Captum: A unified and generic model interpretability library for PyTorch, September 2020.
- [15] Aditi S. Krishnapriyan, Amir Gholami, Shandian Zhe, Robert M. Kirby, and Michael W. Mahoney. Characterizing possible failure modes in physics-informed neural networks, November 2021. arXiv:2109.01050 [physics].
- [16] Gregory Kang Ruey Lau, Apivich Hemachandra, See-Kiong Ng, and Bryan Kian Hsiang Low. PINNACLE: PINN Adaptive ColLocation and Experimental points selection, April 2024. arXiv:2404.07662 [physics, stat] version: 1.
- [17] Dong C. Liu and Jorge Nocedal. On the limited memory BFGS method for large scale optimization. *Mathematical Programming*, 45(1):503–528, August 1989.
- [18] Lu Lu, Xuhui Meng, Zhiping Mao, and George Em Karniadakis. DeepXDE: A Deep Learning Library for Solving Differential Equations. *SIAM Review*, 63(1):208–228, January 2021.

- [19] V. Medvedev, A. Erdmann, and A. Roskopf. Modeling of Near-and Far-Field Diffraction from EUV Absorbers Using Physics-Informed Neural Networks. In *2023 Photonics & Electromagnetics Research Symposium (PIERS)*, pages 297–305, July 2023. ISSN: 2831-5804.
- [20] Malte Braack And Piotr Boguslaw Mucha. Directional Do-Nothing Condition for the Navier-Stokes Equations. *Journal of Computational Mathematics*, 32(5):507–521, June 2014.
- [21] Adam Paszke, Sam Gross, Francisco Massa, Adam Lerer, James Bradbury, Gregory Chanan, Trevor Killeen, Zeming Lin, Natalia Gimelshein, Luca Antiga, Alban Desmaison, Andreas Köpf, Edward Yang, Zach DeVito, Martin Raison, Alykhan Tejani, Sasank Chilamkurthy, Benoit Steiner, Lu Fang, Junjie Bai, and Soumith Chintala. PyTorch: An Imperative Style, High-Performance Deep Learning Library, December 2019.
- [22] Garima Pruthi, Frederick Liu, Mukund Sundararajan, and Satyen Kale. Estimating Training Data Influence by Tracing Gradient Descent, November 2020. arXiv:2002.08484 [cs, stat].
- [23] M. Raissi, P. Perdikaris, and G. E. Karniadakis. Physics-informed neural networks: A deep learning framework for solving forward and inverse problems involving nonlinear partial differential equations. *Journal of Computational Physics*, 378:686–707, February 2019.
- [24] M. Schäfer, S. Turek, F. Durst, E. Krause, and R. Rannacher. Benchmark Computations of Laminar Flow Around a Cylinder. In Ernst Heinrich Hirschel, Kozo Fujii, Bram Van Leer, Michael A. Leschziner, Maurizio Pandolfi, Arthur Rizzi, Bernard Roux, and Ernst Heinrich Hirschel, editors, *Flow Simulation with High-Performance Computers II*, volume 48, pages 547–566. Vieweg+Teubner Verlag, Wiesbaden, 1996. ISBN 978-3-322-89851-7 978-3-322-89849-4. Series Title: Notes on Numerical Fluid Mechanics (NNFM).
- [25] Sifan Wang, Yujun Teng, and Paris Perdikaris. Understanding and mitigating gradient pathologies in physics-informed neural networks, January 2020. arXiv:2001.04536 [cs, math, stat].
- [26] Sifan Wang, Xinling Yu, and Paris Perdikaris. When and why PINNs fail to train: A neural tangent kernel perspective. *Journal of Computational Physics*, 449:110768, January 2022.
- [27] Sifan Wang, Shyam Sankaran, Hanwen Wang, and Paris Perdikaris. An Expert’s Guide to Training Physics-informed Neural Networks, August 2023. arXiv:2308.08468 [physics].
- [28] Sifan Wang, Shyam Sankaran, and Paris Perdikaris. Respecting causality for training physics-informed neural networks. *Computer Methods in Applied Mechanics and Engineering*, 421:116813, March 2024.

## A Appendix / Supplemental Material

### A.1 Influence Functions

In this part, we aim to formulate the key steps for influence functions [8] and adjust them for the application to PINNs. Therefore, we will slightly generalize the results from [12; 13]. Thereby, we will provide proofs for the statements from Section 2. We start with a well-known result [5], which is the crucial ingredient for influence functions.

**Lemma 1** (‘argmin’-trick). *Let  $g : \Theta \times U \rightarrow \mathbb{R}$ , with  $\Theta \subset \mathbb{R}^P$  convex, compact and  $U \subseteq \mathbb{R}$ , be a function, which is twice continuously differentiable w.r.t.  $\theta \in \Theta$  and continuously differentiable w.r.t.  $\epsilon \in U$ . Furthermore, we assume that  $g$  has a positive definite Hessian matrix<sup>1</sup>  $H_\theta := \nabla_\theta^2 g(\theta, \epsilon)$  for all  $\epsilon \in U$ . Then  $h(\epsilon) := \arg \min_{\theta \in \Theta} g(\theta, \epsilon)$  is unique, and its derivative is given by*

$$\frac{\partial h(\epsilon)}{\partial \epsilon} = -H_\theta^{-1} \cdot \frac{\partial}{\partial \epsilon} \nabla_\theta g(\hat{\theta}, \epsilon) \quad . \quad (7)$$

where  $\hat{\theta} := h(\epsilon)$  denotes the minimum.

*Proof.* Since the Hessian is positive definite,  $g(\theta, \epsilon)$  is strictly convex w.r.t.  $\theta$  for any  $\epsilon \in U$ . Further, any continuous function on a compact domain has a minimum (extreme value theorem). Due to the strict convexity, this minimum will be unique  $\hat{\theta} = h(\epsilon)$  for any given  $\epsilon$ . At the minimum we will have

$$\nabla_\theta g(\hat{\theta}, \epsilon) = 0 \quad . \quad (8)$$

---

<sup>1</sup>Note, that any function with a positive definite Hessian is strictly convex, but the converse does not necessary hold.

A derivative of Eq. (8) w.r.t.  $\epsilon$  leads to

$$0 = \nabla_{\hat{\theta}}^2 g(\hat{\theta}, \epsilon) \cdot \frac{\partial h(\epsilon)}{\partial \epsilon} + \frac{\partial}{\partial \epsilon} \nabla_{\hat{\theta}} g(\hat{\theta}, \epsilon) \quad . \quad (9)$$

Since the Hessian is positive definite, we can invert the Hessian and a simple rearrangement of Eq. (9) shows the assertion.  $\square$

By means of this result, we can approximate how an arbitrary function, depending on the optimal parameters  $\hat{\theta}$ , changes when adding and removing points to our training set.

**Proposition 1.** Consider a total loss function  $\mathcal{L}(\mathcal{X}; \theta) = \frac{1}{N} \sum_{i=1}^N L(\mathbf{x}_i; \theta)$  with training points  $\mathcal{X} = \{\mathbf{x}_1, \dots, \mathbf{x}_N\}$ , and denote by  $\mathcal{X}^- = \{\mathbf{x}_1^-, \dots, \mathbf{x}_{m^-}^-\} \subseteq \mathcal{X}$  training points we want to remove and by  $\mathcal{X}^+ = \{\mathbf{x}_1^+, \dots, \mathbf{x}_{m^+}^+\}$  training points we want to add. We will assume that  $\mathcal{L}$  has a positive definite Hessian matrix  $H_{\hat{\theta}} = \nabla_{\hat{\theta}}^2 \mathcal{L}(\mathcal{X}; \theta)$ . Furthermore, let  $f : \Omega \times \Theta \rightarrow \mathbb{R}$  be an arbitrary function, depending on the parameters  $\theta \in \Theta$  and being twice continuously differentiable w.r.t.  $\theta \in \Theta$ . Then the effect of adding and removing training points on the function  $f$  can be approximated by

$$f(\mathbf{z}; \hat{\theta}) - f(\mathbf{z}; \hat{\theta}_{\mathcal{X}^+, \mathcal{X}^-}) = \frac{1}{N} \text{Inf}_{f(\mathbf{z}; \hat{\theta})}(\mathcal{X}^+, \mathcal{X}^-) + \mathcal{O}(N^{-2}) \quad (10)$$

where  $\hat{\theta}$  are the optimized parameters of the original model with training points  $\mathcal{X}$  and  $\hat{\theta}_{\mathcal{X}^+, \mathcal{X}^-}$  the optimized parameters for training points  $\mathcal{X} \cup \mathcal{X}^+ \setminus \mathcal{X}^-$ .  $\text{Inf}_{f(\mathbf{z}; \hat{\theta})}$  is the so-called influence function, which is defined by

$$\text{Inf}_{f(\mathbf{z}; \hat{\theta})}(\mathcal{X}^+, \mathcal{X}^-) := \sum_{i=1}^{m^+} \text{Inf}_{f(\mathbf{z}; \hat{\theta})}(\mathbf{x}_i^+) - \sum_{i=1}^{m^-} \text{Inf}_{f(\mathbf{z}; \hat{\theta})}(\mathbf{x}_i^-) \quad (11)$$

$$\text{with } \text{Inf}_{f(\mathbf{z}; \hat{\theta})}(\mathbf{x}_i) := \nabla_{\hat{\theta}} f(\mathbf{z}; \hat{\theta}) \cdot H_{\hat{\theta}}^{-1} \cdot \nabla_{\hat{\theta}} L(\mathbf{x}_i; \hat{\theta}) \quad . \quad (12)$$

*Proof.* The optimal parameter under the influence of adding and removing points, is given as

$$\hat{\theta}_{\epsilon, \mathcal{X}^+, \mathcal{X}^-} := \arg \min_{\theta \in \Theta} \left[ \frac{1}{N} \sum_{i=1}^N L(\mathbf{x}_i; \theta) + \epsilon \sum_{i=1}^{m^+} L(\mathbf{x}_i^+; \theta) - \epsilon \sum_{i=1}^{m^-} L(\mathbf{x}_i^-; \theta) \right] \quad , \quad (13)$$

where  $\hat{\theta}_{0, \mathcal{X}^+, \mathcal{X}^-} = \hat{\theta}$  is the optimized parameter for the training set  $\mathcal{X}$ . As we can multiply the inner function of Eq. (13) by any positive number without changing  $\hat{\theta}_{\epsilon, \mathcal{X}^+, \mathcal{X}^-}$ , the optimal parameter for the training set  $\mathcal{X} \cup \mathcal{X}^+ \setminus \mathcal{X}^-$  is  $\hat{\theta}_{1/N, \mathcal{X}^+, \mathcal{X}^-} = \hat{\theta}_{\mathcal{X}^+, \mathcal{X}^-}$ . Therefore, we will consider

$$\begin{aligned} \frac{f(\mathbf{z}; \hat{\theta}) - f(\mathbf{z}; \hat{\theta}_{\epsilon, \mathcal{X}^+, \mathcal{X}^-})}{\epsilon} &= - \left. \frac{\partial f(\mathbf{z}; \hat{\theta}_{\epsilon, \mathcal{X}^+, \mathcal{X}^-})}{\partial \epsilon} \right|_{\epsilon=0} + \mathcal{O}(\epsilon) \\ &= - \nabla_{\hat{\theta}} f(\mathbf{z}; \hat{\theta}) \cdot \left. \frac{\partial \hat{\theta}_{\epsilon, \mathcal{X}^+, \mathcal{X}^-}}{\partial \epsilon} \right|_{\epsilon=0} + \mathcal{O}(\epsilon) \\ &= \nabla_{\hat{\theta}} f(\mathbf{z}; \hat{\theta}) \cdot H_{\hat{\theta}}^{-1} \cdot \nabla_{\hat{\theta}} \left( \sum_{i=1}^{m^+} L(\mathbf{x}_i^+; \hat{\theta}) - \sum_{i=1}^{m^-} L(\mathbf{x}_i^-; \hat{\theta}) \right) + \mathcal{O}(\epsilon) \end{aligned} \quad (14)$$

where we used Taylor's theorem in the first step and Lemma 1 in the last step.  $\square$

Note, that the loss function will not be strictly convex in the most approaches, which implies, in particular, that it will not have a positive definite Hessian. However, in a progressing training, we can always restrict the possible parameter set  $\Theta$  in a meaningful way, such that the loss function is strictly convex and having a positive definite Hessian.

Therefore, the influence function will approximate the change of a function  $f(\mathbf{z}; \hat{\theta})$ , when retraining it on a different training set. Usually, one uses the loss itself  $f(\mathbf{x}_{\text{test}}; \hat{\theta}) = L(\mathbf{x}_{\text{test}}; \hat{\theta})$  on a test point for that function. However, we can also study the influence to physical observables, which are relevant for the considered problem. Since, we can also study the influence to mean values, we can therefore study also the influence to regions in our domain.

In analogous fashion, we can easily extend this framework to study the effect of upweighting or downweighting individual loss terms. This is in particular interesting for PINNs, since a wrong weighting of the loss terms, is known to reduce the accuracy of PINNs drastically [25].

**Corollary 1.** Consider a total loss, which is built by several loss terms  $\mathcal{L}_j$

$$\mathcal{L}(\mathcal{X}; \theta) = \sum_{j=1}^k \mathcal{L}_j(\mathcal{X}; \theta) = \frac{1}{N} \sum_{i=1}^N \sum_{j=1}^k l_j(\mathbf{x}_i; \theta) \quad . \quad (15)$$

The procedure of removing the loss terms  $\mathcal{L}_j$  with  $j \in K^- \subsetneq \{1, \dots, k\}$  can be approximated by

$$f(\mathbf{z}; \hat{\theta}) - f(\mathbf{z}; \hat{\theta}_{K^-}) = \frac{1}{N} \text{Inf}_{f(\mathbf{z}, \hat{\theta})}(K^-) + \mathcal{O}(N^{-2}) \quad (16)$$

where  $\hat{\theta}$  is the optimized parameter of the original model and  $\hat{\theta}_{K^-}$  is the optimized parameter for the model with removed losses terms and

$$\text{Inf}_{f(\mathbf{z}, \hat{\theta})}(K^-) := - \sum_{j \in K^-} \nabla_{\hat{\theta}} f(\mathbf{z}; \hat{\theta}) \cdot H_{\hat{\theta}}^{-1} \cdot \nabla_{\hat{\theta}} \mathcal{L}_j(\mathcal{X}; \hat{\theta}) \quad . \quad (17)$$

*Proof.* Analogous, to Proposition 1 we will define

$$\hat{\theta}_{\epsilon, K^-} := \arg \min_{\theta \in \Theta} \left[ \frac{1}{N} \sum_{i=1}^N \sum_{j=1}^k l_j(\mathbf{x}_i; \theta) - \epsilon \sum_{i=1}^N \sum_{j \in K^-} l_j(\mathbf{x}_i; \theta) \right] \quad (18)$$

as the optimal parameter, which will remove the loss terms  $\mathcal{L}_j$  with  $j \in K^-$  for  $\epsilon = 1/N$ . The assertion follows with the analogue steps above.  $\square$

## A.2 Navier-Stokes Parametrization

The rectangular cavity characterizing the 2D Navier-Stokes problem formulation is given in Table 2.

Table 2: Geometric Parameters of the Cavity

Parameter	Value [m]
$x_{\min}$	0
$x_{\max}$	2.2
$y_{\min}$	0
$y_{\max}$	0.41
Cylinder radius	0.05
Cylinder position $(x_c, y_c)$	(0.2, 0.2)

The parabolic inflow is defined as

$$\mathbf{u}(x_{\min}, y) = \begin{pmatrix} U_{\max} y \frac{y_{\max} - y}{y_{\max}^2} \\ 0 \end{pmatrix}, \quad (19)$$

where  $U_{\max} = 0.3$  m/sec. Furthermore, the fluid density  $\rho$  was set to 1 and the kinematic viscosity  $\nu$  to 0.001.

### A.3 Supplemental Figures

Figure 4 is supplementary to Figure 1 and shows the model predictions additionally for  $\|\mathbf{u}\|$  and for  $\phi_{\text{broken}}$ ,  $\phi_{\text{bad}}$  as well as target values precomputed with the finite element method (FEM) program FEniCS sourced from [27].

Figure 5 shows the absolute errors between model predictions and the target values depicted in Figure 4d. Note that  $\phi_{\text{broken}}$  is evaluated against correct target values.

Figure 6 shows the influence heatmap produced by  $\phi_{\text{broken}}$  and  $\phi_{\text{bad}}$  for the same training point as used in Figure 2.

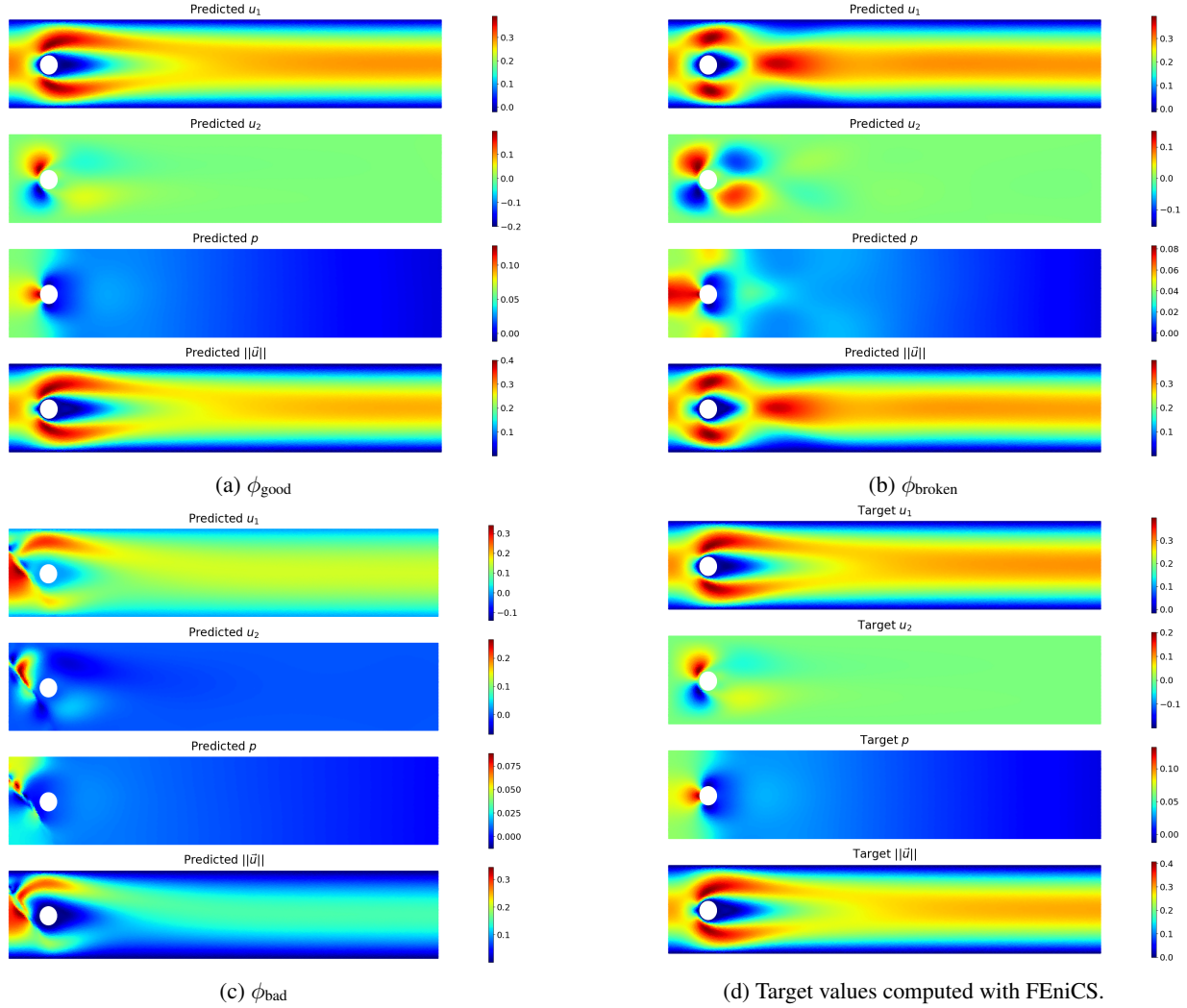


Figure 4: Trained models and target values with respective predictions:  $u_1$ ,  $u_2$ ,  $p$ ,  $\|\mathbf{u}\|$  (top to bottom).

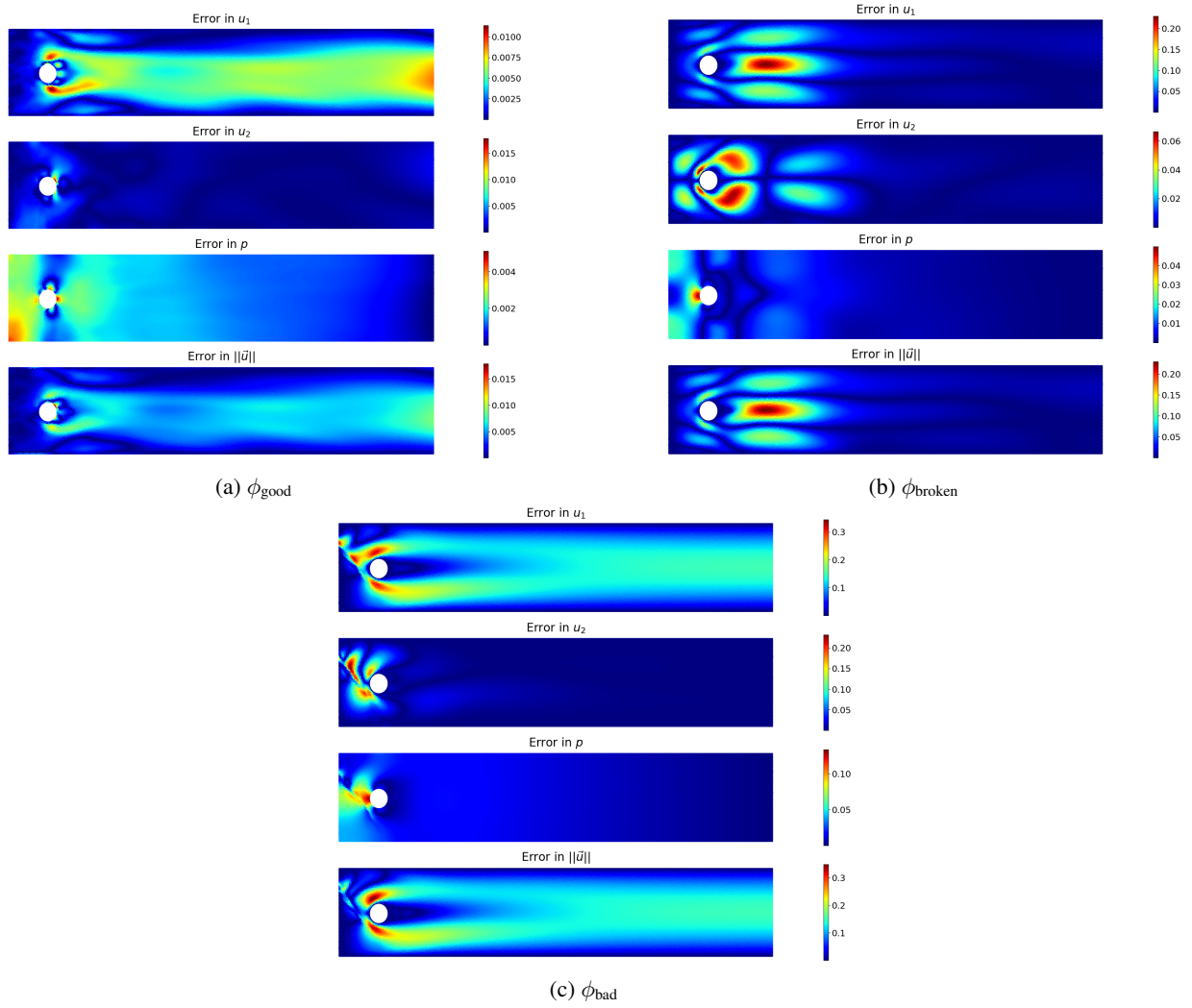


Figure 5: Absolute errors between respective model predictions for each output dimension w.r.t. precomputed target values.

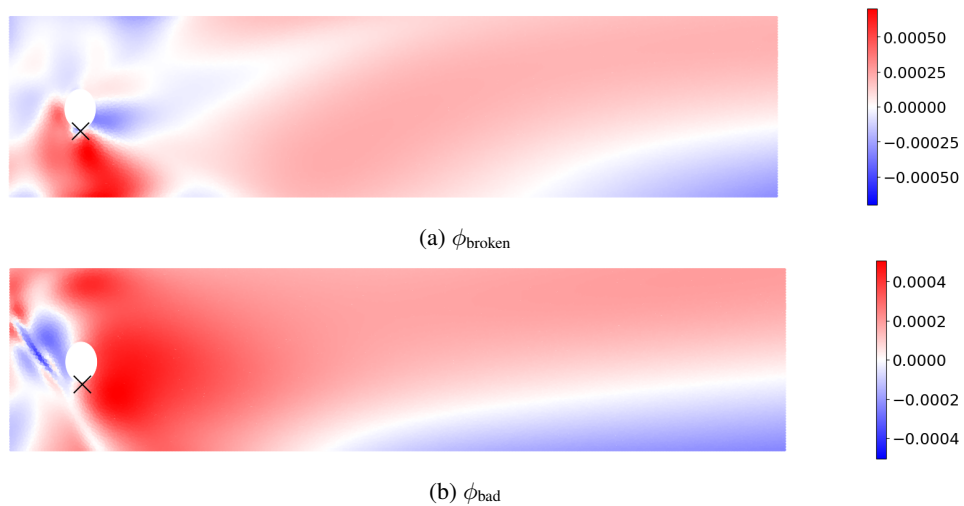


Figure 6: Influence heatmaps on the prediction of  $u_1$  of a single training point close to the cylinder (bottom).